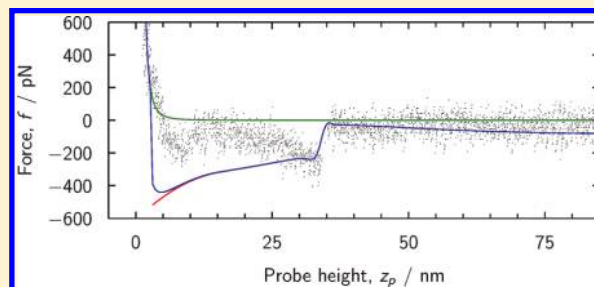


Pulling Nanotubes from Supported Bilayers

Jonathan W. Armond,^{†,‡,§} Julie V. Macpherson,[‡] and Matthew S. Turner^{*,†}[†]Department of Physics, [‡]Department of Chemistry, and [§]MOAC DTC, University of Warwick, Coventry, CV4 7AL, U.K.

ABSTRACT: The force required to form a nanoscale tube from a supported lipid bilayer (SLB) by pulling was measured using an atomic force microscope (AFM). The equilibrium membrane shape during an AFM pulling experiment was calculated and used to derive a general force–distance relationship for pulling a tube from an SLB. We compare these theoretical results with our experimental data and determine the tube radius, the force required to elongate the tube, and, consequently, the surface tension. For a dioleoylphosphatidylcholine (DOPC) SLB, the tension was found to be close to membrane rupture during the pulling experiment.



INTRODUCTION

Nanotubes, on the order of tens of nanometers in diameter, formed from lipid membranes are important in a number of contexts. For example, kidney cells are able to deform their membranes to form tubes that can connect to the membranes of other cells and be used to transfer material between them.^{1,2} Lipid tubes have also been observed to connect, and facilitate communication between immune cells.^{3,4} In particular, the HIV-1 virus can spread through tube interconnections between T-cells.⁵ Prions can also travel between infected and noninfected cells through lipid tubes.⁶ It has been proposed that diffusion of membranes protein on such nanotubes could provide a method to directly test the predictions of the Saffman–Delbruck theory of membrane diffusion.⁷ Here, we show that, by forming and pulling a nanotube from the surface of a supported lipid bilayer (SLB), it is possible to measure bilayer surface tension.

Experimentally, *in vitro* model membrane tubes have been produced by the application of a localized force. These differ from biological membranes, which are filled with actin and differ compositionally. This has been demonstrated on lipid vesicles using optical tweezers,^{8,9} and by the action of purified kinesin motors.^{10,11} Long-range attractive forces have been observed in atomic force microscopy (AFM) experiments, which may indicate the existence of a lipid tube between probe and surface, on surface SLBs.^{12,13} We present AFM force curve data that demonstrate the formation of membrane tubes from an SLB, and make comparisons with theoretically predicted force curves in an attempt to derive new quantitative information from the data.

Previous theoretical work^{14,15} has modeled an experiment where a force f acting through a point pulls on a vesicle membrane up to a height z_p . During this procedure, the membrane shape is initially in a catenoid-like shape for small z_p , but for larger extensions a discontinuous transition in shape takes place as the membrane relaxes into a tube of radius r_0 with a catenoid-like membrane part at its base and a closed surface at its tip. A tube is formed once the force barrier f_b between the two shapes is overcome; the tube can then be extended at constant force f_0 .

However, if the membrane is attached over a finite (circular) area, with radius r_p , to the force probe, as is the case for vesicle experiments, the magnitude of f_b has been predicted to increase with r_p .⁸ The radius of the initial deformation at the vesicle surface was here assumed to be fixed.

In the present work, we present force data for an AFM experiment, depicted in Figure 1, that involves pulling a membrane tube from an SLB, rather than a vesicle, using a large-surface-area AFM probe. We compare our data with a theoretical prediction of the membrane force corresponding to the membrane shape that minimizes the total energy. As shown in Figure 1, the probe radius can be much larger than the equilibrium tube radius $r_p \gg r_0$, and, crucially, the radius of the patch of membrane detached from the surface r_f can vary. The surface tension σ is controlled by the interaction between the bilayer membrane and the supporting surface. An SLB presents some advantages over vesicles for this experiment, in particular the surface tension is fixed and not determined by pressure difference as for the vesicle. Furthermore, SLBs have potential applications as, e.g., biosensors.¹⁶

MEMBRANE THEORY

The free energy of a membrane according to the Canham–Helfrich model^{17,18} is

$$F = \int \left[\frac{\kappa}{2} (2H)^2 + \sigma \right] dA - P \int dV \quad (1)$$

where $2H$ is the mean curvature, κ is the elastic bending modulus, and P is the pressure across the membrane. We have assumed that the bilayer is symmetric and therefore has no spontaneous curvature, and that Gaussian curvature can be neglected since no topological changes take place. In the following we make the

Received: February 18, 2011

Revised: May 31, 2011

Published: June 08, 2011

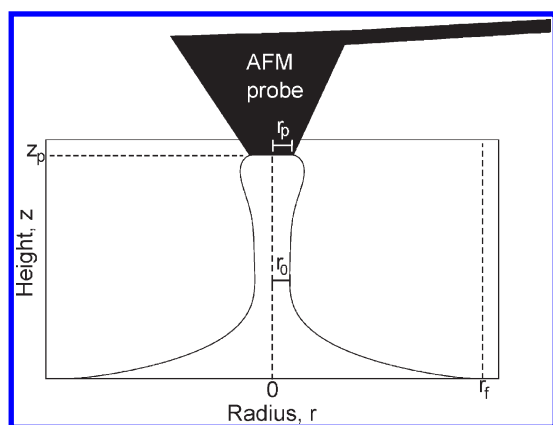


Figure 1. Experimental setup and coordinate system for an AFM lipid tube forming and pulling experiment. The membrane is attached to a flat probe of radius r_p and pulled to a height z_p . Due to the force exerted by the retraction of the probe, some of the membrane, up to radius r_f , is peeled away from the surface.

further assumption that the pressure difference between the outside and inside of the membrane tube is equilibrated, and consequently set $P = 0$. Minimization of this free energy for a cylindrical membrane gives the well-known equilibrium tube radius $r_0 = (\kappa/2\sigma)^{1/2}$. Thus perfectly cylindrical (long) tubes extend at constant force $f_0 = 2\pi(2\sigma\kappa)^{1/2}$. Consequently, after the membrane has been pulled to a sufficient height, we would expect the pulling force f to approach f_0 , because the membrane shape near the AFM probe or surface will have stabilized, and further changes correspond to elongation of the tube.

Equation 1 can be solved variationally, and by assuming axisymmetry, yields a third-order ordinary differential equation (ODE) describing the equilibrium shape of a one-dimensional contour representing the angle of the membrane to the horizontal ψ as a function of arc length s ^{19,20}

$$\begin{aligned} \frac{d^3\psi}{ds^3} = & -\frac{1}{2}\left(\frac{d\psi^3}{ds}\right) - \frac{2\cos\psi}{r}\frac{d^2\psi}{ds^2} + \frac{3\sin\psi}{2r}\left(\frac{d\psi^2}{ds}\right) \\ & + \frac{3\cos^2\psi - 1}{2r^2}\frac{d\psi}{ds} + \frac{d\psi}{ds}\bar{\sigma} - \frac{(\cos^2\psi + 1)\sin\psi}{2r^3} \\ & + \frac{\bar{\sigma}\sin\psi}{r} - \bar{P} \end{aligned} \quad (2)$$

where $\bar{\sigma} = \sigma/\kappa$ and $\bar{P} = P/\kappa$.

This contour, rotated around the pulling axis, represents the three-dimensional membrane shape. To solve (eq 2) boundary conditions must be applied. Mimicking the AFM experiment, we fix the membrane to the surface and to the probe, with zero curvature at these points ($\psi'(r_p) = \psi'(r_f) = 0$), and clamp the radius at which the membrane leaves the surface at r_f ($z = 0$ at $r = r_f$ as in Figure 1). In our formalism, only the membrane that has left the surface contributes to the free energy F , although the tension is set by the reservoir that remains in contact with the surface. We take $P = 0$, corresponding to a quasi-equilibrium pulling experiment such that the fluid has time to fill any increased membrane volume. In the experiments, this condition will be shown by an absence of pulling velocity-dependent components.

We used the ODE analysis software AUTO 2007p²¹ to numerically solve (eq 2) for the membrane shape. By performing a continuation process to vary the parameters z_p and r_f we were

able to follow the membrane shape transition during the tube formation process. Note that the membrane shape, and therefore r_f and its surface area, has an effect on the free energy, hence the contribution involving σ . In general, σ will be different from that of a vesicle, as it is fixed by a surface interaction energy, that we assume to be constant. Thus the effect of increasing r_f involves paying a free energy cost for “peeling” the membrane off the surface. This is captured through the change in energy (area) of the unbound membrane. For each value of z_p during the *in silico* pulling experiment, r_f was calculated by finding the global minimum of the free energy obtained by solving (eq 2) over a range of r_f .

MATERIALS AND METHODS

AFM Pulling Experiment. Force–Extension curves were measured for SLBs composed of dioleoylphosphatidylcholine (DOPC). These were prepared on freshly cleaved mica surfaces by deposition of extruded unilamellar vesicles.²² Briefly, DOPC (Avanti Polar-Lipids, Alabaster, AL) was suspended in HEPES buffer (150 mM NaCl, 3 mM NaN₃, 10 mM HEPES, pH 7.4) to 1 mg/mL, and subjected to repeated freeze/thaw cycles to produce unilamellar vesicles. These were then extruded through a 100 nm pore polycarbonate membrane using a Liposofast extrusion device (Avestin Inc., Canada) to produce uniform size vesicles. Muscovite mica was cleaved to produce fresh, flat surfaces (rms roughness <1 nm, imaged by AFM) before deposition of ~ 30 L of vesicle solution, which was covered with a Petri dish to avoid evaporation and left to form a bilayer for ~ 30 min. Before making force measurements, samples were imaged by AFM to check that smooth bilayers had been produced.

A previous force-curve study on deposited unilamellar vesicles, aimed at studying bilayer fusion, reported considerable variation using standard probes,¹³ probably due to the high curvature; hence we sought to increase reproducibility by flattening the sharp probe to fabricate a large surface area probe with larger r_p . The AFM probe (NP, Veeco, USA; nominal radius of curvature 20 nm) was scanned on a rough diamond surface at a force > 1 N with a scan size of $40 \text{ m} \times 40 \text{ m}$ and scan rate of 60 Hz for 15 min (based on a protocol by Whisman et al.²³). After this procedure, the probe was noticeably more blunt as assessed by imaging a sharp-spike sample (TGX01, NT-MDT Europe BV, The Netherlands) and had an approximate radius of curvature of 100 nm.

During a measurement cycle, the AFM probe was moved toward the surface until the force reached a large repulsive force but without rupturing the bilayer (20 nN was found to be suitable), held in place for 1 s, and then retracted at constant velocity. To keep dynamic effects at a minimum, retraction velocities were chosen to be as slow as possible while also being fast enough to avoid thermal drifts; we compared the results for two velocities $v = 500$ and 250 nm/s. The deflection of the cantilever is directly proportional to the force at the probe by Hooke’s law $f = kx$, where k is the spring constant of the cantilever. For each cantilever, k was calculated from the thermal noise power spectrum.²⁴ Due to the stochastic nature of the experiment, not all force curves show all features; curves were manually classified according to feature and further analysis of each feature performed on each set. The position and magnitudes of peaks and steps in the force curves was automatically determined using purpose-built software written in Python. Peaks were identified using a continuous wavelet transform (CWT) algorithm based on one proposed for the analysis of mass

spectrometry data.²⁵ Briefly, the CWT is computed over the region of interest of the curve at multiple scales using a “differentiated Gaussian” wavelet of order 4. Local maxima at each scale are identified using a sliding window. The local maxima are then connected between scales to form ridges using distance and gap thresholding. The peak strength of each sufficiently long ridge is estimated, and those with signal-to-noise ratios larger than some threshold are identified as peaks. Error bounds shown on means are sample standard deviations.

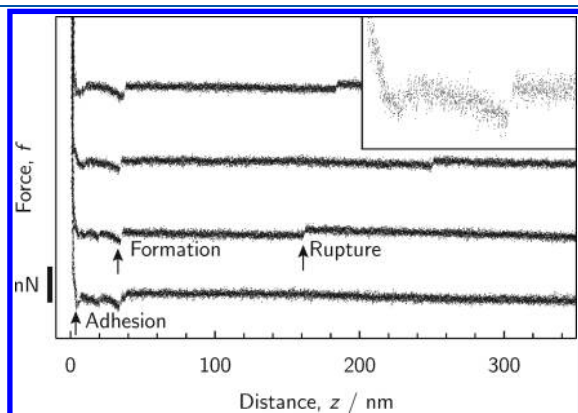


Figure 2. Typical retract force curves. Three characteristic features appear on these curves, which may be attributable to adhesion, tube formation, and tube rupture. Arrows show (from left to right) an adhesion feature, a formation feature, and a tube rupture feature. Inset shows the first 50 nm. Curves are offset in the vertical direction for clarity. Retraction velocity was $v_p = 500$ nm/s.

RESULTS

Force measurements were repeated several hundred times at each velocity at the same location. In the following, we only examine the retraction curve, as this is most relevant to tube formation. A selection of typical retraction force curves showing the reproducible features (occurring in >25% of curves) is shown in Figure 2 with the features marked by arrows. We propose that these features correspond to adhesion, formation of membrane tube, and rupture of tube (arrows in Figure 2, from left-to-right). These are discussed in the following sections.

Adhesion. Around half of the forces curves show an attractive force at very small distance from the surface that is variable in magnitude. On the basis of the short-range of this force, we suggest this peak is due to bilayer adhesion to the underlying mica support. Pulling at 500 nm/s, the mean force is 164 ± 115 pN and arises at a mean distance of 7.8 ± 1.4 nm ($n = 227$). When pulling at a slower speed (250 nm/s), the range of the force remains roughly constant, with a mean distance at 8.1 ± 1.5 nm, but the mean force is reduced to 112 ± 109 pN ($n = 71$) (see histograms in Figure 3). A loading rate-dependent force is consistent with a “bond-breaking” transition, such as an adhesion.²⁶

Tube Formation. The second feature indicated in Figure 2 occurs at a reproducible distance several times the thickness of a bilayer (around 5 nm).²² The mean peak force attributed to tube formation was 115 ± 105 pN, encountered at a mean distance of 31.3 ± 2.1 nm from surface contact ($n = 63$) for a retraction velocity of 500 nm/s. For the slower velocity 250 nm/s, the force was 79 ± 162 pN at an average distance of 34.0 ± 10.6 nm ($n = 25$) (see Figure 3). Although the mean peak force at the slower velocity is less than that at the faster velocity,

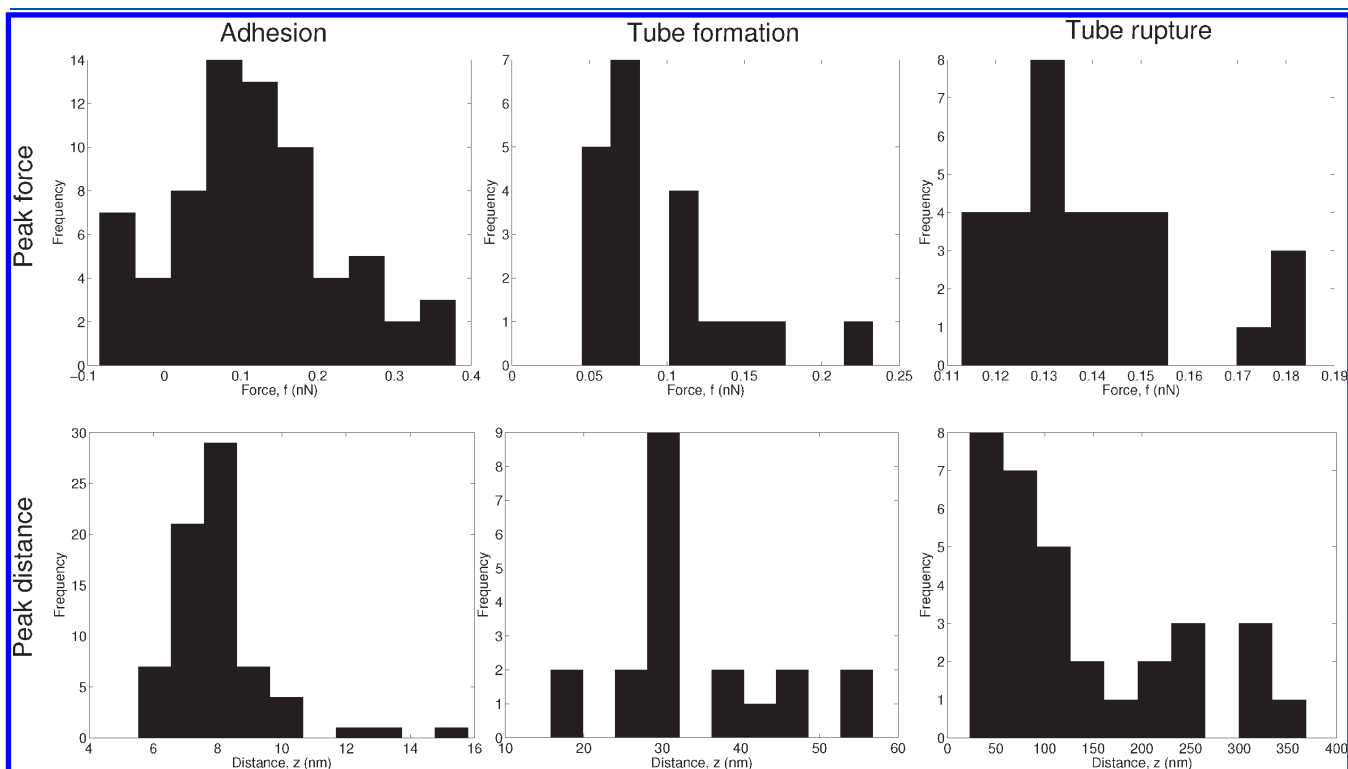


Figure 3. Peak force (upper) and distance (lower) histograms for (left) adhesion ($n = 227$), (middle) tube formation ($n = 63$), and (right) tube rupture ($n = 122$). Retract rate was $v_p = 500$ nm/s. Mean forces were 164 ± 115 pN, 115 ± 105 pN, and 132 ± 57 pN for adhesion, tube formation, and tube rupture, respectively. Mean distances were 7.8 ± 1.4 nm, 31.3 ± 2.1 nm, and 139.6 ± 97.3 nm for adhesion, tube formation, and tube rupture, respectively. (\pm S.D.).

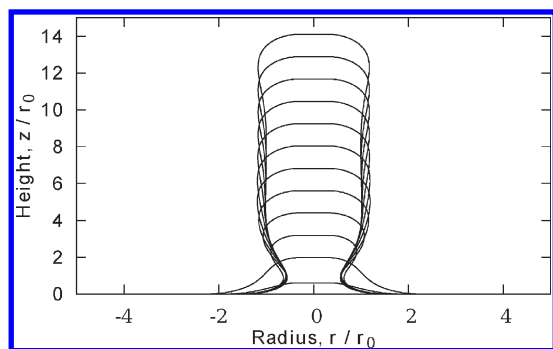


Figure 4. Sequence of membrane shapes during pulling. The solution of the shape equation for a range of z_p shows the catenoid-like solution at small z_p with large r_f and the tube solution at larger z_p with $r_f = r_0$.

taking into account the error bounds, they are not inconsistent with each other, lending support to the hypothesis that dissipation is not a significant effect at these velocities. Moreover, theoretically predicted force curves point to a well-defined tube formation transition accompanied by a step in force (see later section Theoretical Force Curve), suggesting that this peak is due to tube formation.

Tube Rupture. Often, a step reduction to zero attractive force appears at some larger, variable distance from the surface. The mean distance at which the step occurred was similar at both pulling rates (*t*-test on log-transformed data, $p = 0.69$); 139.6 ± 97.3 nm for velocity 500 nm/s ($n = 122$) and 133.0 ± 99.4 nm for pulling velocity 250 nm/s ($n = 32$). The mean force magnitude of the steps was also not significantly variable (*t*-test on log-transformed data, $p = 0.16$); 132 ± 57 pN at 500 nm/s, and 140 ± 18 pN at 250 nm/s (see Figure 3).

The most ready explanation for a sudden drop in force, if a tube has been formed, is the tube either ruptures or detaches from the probe. Assuming this to be the case, and that the force after the step is zero, as was confirmed by withdrawing the probe to large distances (~ 5 m), then the magnitude of the jump f_r is equal to the tube extension force $f_0 = 2\pi(2\sigma\kappa)^{1/2}$.

A single rupture was seen in 27% of retractions at 500 nm/s. Occasionally, the force step was repeated twice. Assuming the number of tubes formed n to be Poisson distributed the mean number of tubes is $\bar{n} = \log \text{Prob}(n = 0) = 0.33$. The mean step force of second steps was 127 ± 9 pN, with mean distance 167.7 ± 20.1 nm, at a pulling velocity of 500 nm/s. Two steps were observed together in 4.1% of retractions at this velocity, in close agreement with the expected number based on the Poisson distribution 3.8%. At a pulling velocity of 250 nm/s, two steps were observed in only 1.6% of retractions. The mean force of the second step, at this velocity, was 135 ± 4 pN, with mean distance 201.0 ± 79.9 nm. This may be attributable to multiple tubular connections between probe and surface, as suggested by Maeda et al.¹²

Theoretical Force Curve. The force curve can also be estimated theoretically, and this estimate can be compared to the experimental data. To achieve this, for each probe height we minimized the free energy of the membrane shape (eq 1) using a variational method. We present our results in dimensionless units, scaled by the natural units of length r_0 and force f_0 . The probe patch radius r_p remains an independent parameter. Here we used $\kappa = 85$ pN nm²⁷ and fitted the resulting curves to data to determine σ .

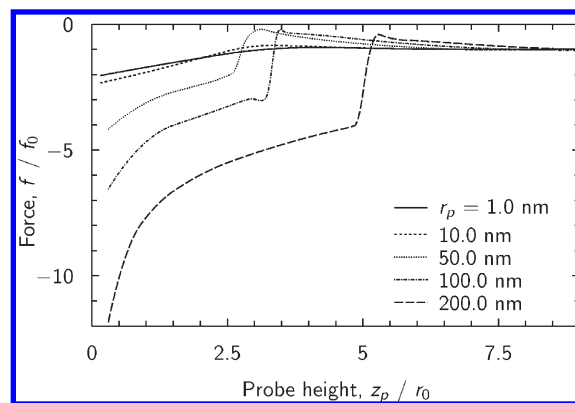


Figure 5. Force at probe as z_p during pulling experiment, obtained by differentiating the free energy F with respect to z_p . For $r_p \geq r_0$, the tube formation is apparent as a rapid decrease in force. Negative force denotes an attractive force, that is, resisting the retraction of the probe.

Solutions of eq 2 for increasing probe height z_p and various probe radii r_p are shown in Figure 4. The surface detachment radius r_f is determined for each solution by minimizing the free energy. Each pull begins by forming a “tent”-like shape. This is characterized by a large surface radius r_f . After reaching a height particular to the probe radius, the surface radius drops, and a tube begins to form with radius r_0 . When $r_p \gg r_0$, this drop is rapid. Further increase in height extends the tube, and no further shape changes take place. The force increases immediately after tube formation, reaching an asymptotic value of $f^\infty = f_0$.

The force profile as z_p is increased, calculated by differentiating the free energy obtained for a sequence of shapes with respect to z_p , is shown in Figure 5 and is analogous to a force curve obtained using AFM. In the force curve the transition between “tent”-like and tubular is clearly visible as a sharp step to lower attractive force, for sufficiently large probes $r_p > r_0$.

Assuming that the mean tube rupture force (132 ± 57 pN), which manifests as a simple step down to zero force from a constant force, corresponds to the tube elongation force, it is possible to estimate the surface tension. Using $f_0 = 2\pi(2\sigma\kappa)^{1/2}$, and the rigidity $\kappa = 85$ pN·nm for DOPC,²⁷ we find $\sigma_1 = 2.7 \pm 0.1$ pN/nm.

Another independent estimate of the surface tension can be obtained through the highly repeatable distance at which the tube formation feature was observed by using this distance to define the length scale r_0 in the theoretically calculated force curves shown in Figure 5; a comparison is made in Figure 6. For the probe radii used in the experiment, the theory predicts the jump in force during formation of the tube to occur at $z = 3.4r_0$. Using the data given in Figure 3 fixes $r_0 = 9.8 \pm 7$ nm as the radius of the tube and the length scale. This provides another estimation of the surface tension $\sigma_2 = 0.50 \pm 6$ pN/nm. Together σ_2 and κ give the force scale $f_0 = 58$ pN. This is the tube elongation force and is around half the experimentally determined value 132 ± 0.5 pN at rupture. The tension calculated at rupture σ_1 is more than 5 times higher, and suggests that an increase in tension is the reason for the rupture of the tube. However, since rupture forces are only measured for tubes that rupture, the distribution is skewed toward higher forces.

At very short distances between the probe tip and the surface, the theoretical curve predicts a very high attractive force because the large radius of the probe results in an large increase in detached membrane area over a very short distance. In reality, the

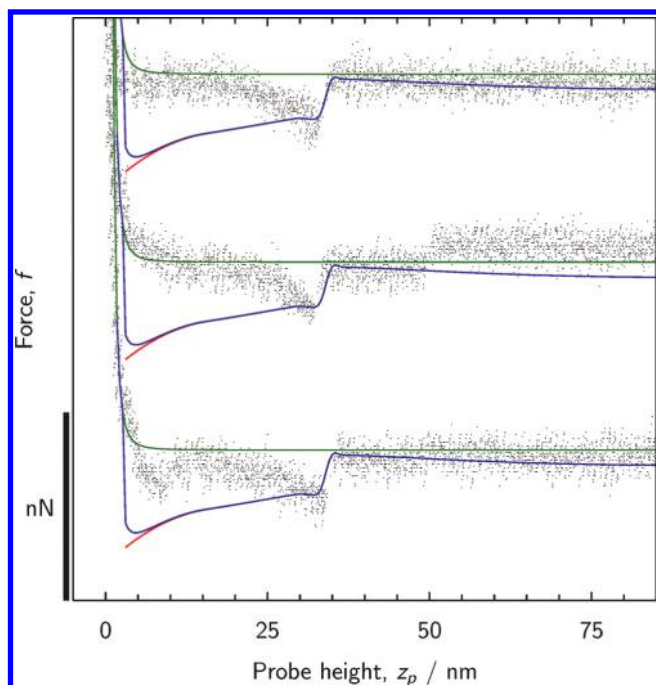


Figure 6. Overlay of theoretical prediction of force during retraction (red lines) on data (black points) showing tube formation feature. The relaxation in force around 30 nm matches well between the theory and data, both in distance and force magnitude. At short distances an additional repulsive force due to bilayer compression arises. The green lines show the form of repulsion that would arise from a Helfrich model that takes into account the suppression of membrane fluctuations in confined (compressed) membranes.²⁸ The blue lines are the resultant (sum of the attraction (red) and Helfrich repulsion (green)), which shows the expected divergent repulsive force as $z_p \rightarrow 0$, as seen in the data. Curves are offset in the vertical direction for clarity. Retraction velocity was $v_p = 500$ nm/s.

compression of the membrane, and entropic contributions due to thermal fluctuations, result in a strong repulsion at short distance.^{29,30} The Helfrich model for the repulsive force due to membrane confinement arises from the corresponding suppression of fluctuations and is plotted in Figure 6 (green lines). We estimate the resultant force to be the sum of the theoretical attraction and the Helfrich repulsion (blue lines). This gives a divergent repulsion, as would ultimately be expected on general grounds when pushing against a solid surface (covered by a SLB). At large distances, the Helfrich force goes to zero and the theoretical attraction asymptotes to f_0 . However, there is still some discrepancy in magnitude of the force at short distance, which is due in part to the fact that the Helfrich model, while analytically soluble, is only a rough approximation to the form of the repulsion. The detachment of the membrane is likely to be a more continuous process than accounted for here, explaining the weaker force observed experimentally. If the process of dewetting of the surface by the membrane was modeled as a continuous function of separation this would effectively tilt the force curve toward positive f at short distances. This may also result in a force increase toward the transition rather than the decrease seen in the data. Finally, the disparity may indicate that $P = 0$ is not a valid assumption and that the pressure is not equilibrating sufficiently fast, particularly at higher retraction velocities. In future work we plan to include these effects.

CONCLUSION

We have shown that pulling tubes from SLBs using AFM is feasible and can be analyzed using equilibrium free energy calculations of membrane shape, as long as attention is restricted to the tube formation transition only. The distance at which tube formation occurs can be used to fix the theoretical length scale and hence calculate the surface tension and tube elongation force. This enables the AFM to be used as an instrument to measure SLB membrane surface tension. The surface tension is likely to be a critically important parameter in designing applications such as biomembrane sensors and has an impact on, e.g., membrane permeability and the stability of embedded membrane proteins. The tension we found for DOPC on mica is close to typical membrane rupture tensions³¹ even just prior to formation, and is much higher at large distance, which suggests that the tube ruptures at large distance, rather than undergoing detachment from the probe. Limitations on the availability of material to form the tube may be a cause of tension increase in this experimental setup.

There were some discrepancies between the theoretically predicted force curve and the AFM curve for short distances. It is possible that a more complete treatment of the bilayer–mica adhesion potential, or the inclusion of a nonzero pressure term, or accounting for interleaflet tension and slipping would,³² improve this agreement. Thus, this work provides a starting point for a more complete theoretical analysis.

In the previous discussion we have not considered dissipation in the membrane. The viscous energy dissipation in the flowing membrane can be estimated to be $dE_m/dt \approx -\eta_m v_p^2$, where $\eta_m = 10^{-10}$ N·s/m is the membrane two-dimensional shear viscosity.²⁹ The contribution to the force from membrane dissipation is then ~ 0.1 fN. There is also a contribution to the force due to dissipation in the flow of the water layer between the membrane and the surface of the order $\eta_w v_p r_0^2/d$, where d is the layer thickness and η_w is the viscosity of water, and is around ~ 0.05 fN. On the scale of forces measured in these experiments, these dissipation effects are negligible. This is in agreement with the observation by Maeda et al. that the features on force curves are not velocity dependent over the range $v_p = 0.5$ – 50 m/s.¹²

AUTHOR INFORMATION

Corresponding Author

*E-mail: m.s.turner@warwick.ac.uk.

ACKNOWLEDGMENT

Part of the equipment used in this research was obtained through Birmingham Science City: Innovative Uses for Advanced Materials in the Modern World (West Midlands Centre for Advanced Materials Project 2), with support from Advantage West Midlands (AWM), and part was funded by the European Regional Development Fund (ERDF). J.W.A. was funded by an EPSRC studentship through the MOAC DTC. M.S.T. acknowledges the support of an EPSRC Leadership Fellowship, Grant Number EP/E501311/1.

REFERENCES

- (1) Rustom, A.; Saffrich, R.; Markovic, I.; Walther, P.; Gerdes, H.-H. *Science* **2004**, *303*, 1007–1010.
- (2) Gerdes, H.-H.; Bukoreshtliev, N. V.; Barroso, J. F. *FEBS Lett.* **2007**, *581*, 2194–2201.

- (3) Önfelt, B.; Nedvetzki, S.; Yanagi, K.; Davis, D. M. *J. Immunol.* **2004**, *173*, 1511–1513.
- (4) Watkins, S. C.; Salter, R. D. *Immunity* **2005**, *23*, 309–318.
- (5) Sowinski, S.; Jolly, C.; Berninghausen, O.; Purbhoo, M. A.; Chauveau, A.; Kohler, K.; Oddos, S.; Eissmann, P.; Brodsky, F. M.; Hopkins, C.; Önfelt, B.; Sattentau, Q.; Davis, D. M. *Nat. Cell Biol.* **2008**, *10*, 211–219.
- (6) Gousset, K.; Schiff, E.; Langevin, C.; Marijanovic, Z.; Caputo, A.; Browman, D. T.; Chenouard, N.; de Chaumont, F.; Martino, A.; Enninga, J.; Olivo-Marin, J.-C.; Mannel, D.; Zurzolo, C. *Nat. Cell Biol.* **2009**, *11*, 328–336.
- (7) Daniels, D. R.; Turner, M. S. *Langmuir* **2007**, *23*, 6667–6670.
- (8) Koster, G.; Cacciuto, A.; Derényi, I.; Frenkel, D.; Dogterom, M. *Phys. Rev. Lett.* **2005**, *94*, 068101.
- (9) Cuvelier, D.; Chiaruttini, N.; Bassereau, P.; Nassoy, P. *Europhys. Lett.* **2005**, *71*, 1015–1021.
- (10) Koster, G.; VanDuijn, M.; Hof, B.; Dogterom, M. *Proc. Natl. Acad. Sci. U.S.A.* **2003**, *100*, 15583–15588.
- (11) Leduc, C.; Campàs, O.; Zeldovich, K. B.; Roux, A.; Jolimaitre, P.; Bourel-Bonnet, L.; Goud, B.; Joanny, J.-F.; Bassereau, P.; Prost, J. *Proc. Natl. Acad. Sci. U.S.A.* **2004**, *101*, 17096–17101.
- (12) Maeda, N.; Senden, T. J.; di Meglio, J.-M. *Biochem. Biophys. Acta, Biomembr.* **2002**, *1564*, 165–172.
- (13) Pera, I.; Stark, R.; Kappl, M.; Butt, H.-J.; Benfenati, F. *Biophys. J.* **2004**, *87*, 2446–2455.
- (14) Derényi, I.; Jülicher, F.; Prost, J. *Phys. Rev. Lett.* **2002**, *88*, 238101.
- (15) Powers, T. R.; Huber, G.; Goldstein, R. E. *Phys. Rev. E* **2002**, *65*, 041901.
- (16) Castellana, E. T.; Cremer, P. S. *Surf. Sci. Rep.* **2006**, *61*, 429–444.
- (17) Canham, P. B. *J. Theor. Biol.* **1970**, *26*, 61–81.
- (18) Helfrich, W. *Z. Naturforsch.* **1973**, *28c*, 693–703.
- (19) Seifert, U.; Bernswald, K.; Lipowsky, R. *Phys. Rev. A* **1991**, *44*, 1182–1202.
- (20) Jülicher, F.; Seifert, U. *Phys. Rev. E* **1994**, *49*, 4728–4731.
- (21) Doedel, E. J.; Champneys, A. R.; Fairgrieve, T. F.; Kuznetsov, Y. A.; Sandstede, B.; Wang, X. *AUTO-07P: Continuation and Bifurcation Software for Ordinary Differential Equations*; Technical Report; Concordia University: Montreal, Canada, 2007.
- (22) Reviakine, I.; Brisson, A. *Langmuir* **2000**, *16*, 1806–1815.
- (23) Whisman, N.; York, D.; Manning, L.; Brant, J.; Dyer, R.; Childress, A.; Marchand, E. A.; Adams, J. D. *Rev. Sci. Instrum.* **2003**, *74*, 4491–4494.
- (24) Hutter, J. L.; Bechhoefer, J. *Rev. Sci. Instrum.* **1993**, *64*, 1868–1873.
- (25) Du, P.; Kibbe, W. A.; Lin, S. M. *Bioinformatics* **2006**, *22*, 2059–2065.
- (26) Merkel, R. *Phys. Rep.* **2001**, *346*, 343–385.
- (27) Rawicz, W.; Olbrich, K.; McIntosh, T.; Needham, D.; Evans, E. *Biophys. J.* **2000**, *79*, 328–339.
- (28) Helfrich, W. *Z. Naturforsch.* **1978**, *33a*, 305–315.
- (29) Das, C.; Khizar, H. S.; Olmsted, P. D.; Connell, S. D. *Phys. Rev. E* **2010**, *82*, 041920.
- (30) Safran, S. A. *Statistical Thermodynamics of Surfaces, Interfaces, and Membranes*; Addison Wesley: Reading, MA, 1994.
- (31) Evans, E.; Heinrich, V.; Ludwig, F.; Rawicz, W. *Biophys. J.* **2003**, *85*, 2342–2350.
- (32) Evans, E.; Yeung, A. *Chem. Phys. Lipids* **1994**, *73*, 39–56.